VIP Lithium-Ion Batteries Very Important Paper

DOI: 10.1002/anie.201407917

Bowl-like SnO_2@Carbon Hollow Particles as an Advanced Anode Material for Lithium-Ion Batteries**

Jin Liang, Xin-Yao Yu, Han Zhou, Hao Bin Wu, Shujiang Ding, and Xiong Wen (David) Lou**

Abstract: *Despite the great advantages of hollow structures as electrodes for lithium-ion batteries, one apparent common drawback which is often criticized is their compromised volumetric energy density due to the introduced hollow interior. Here, we design and synthesize bowl-like SnO_2@carbon hollow particles to reduce the excessive hollow interior space while retaining the general advantages of hollow structures. As a result, the tap density can be increased about 30 %. The as-prepared bowl-like SnO_2@carbon hollow particles with conformal carbon support exhibit excellent lithium storage properties in terms of high capacity, stable cyclability and excellent rate capability.*

As one of the most important energy-storage devices, lithium-ion batteries (LIBs) have been intensively studied in recent years owing to their many merits such as high energy density, environmental benignity, light weight and high power density.[1–5] Although graphite is the dominant anode material for commercial LIBs, its relatively low theoretical capacity (372 $mAh\,g^{-1}$) largely impedes the development of LIBs with high energy density. Numerous efforts have been devoted to search for high-capacity anode materials that can replace graphite.[6–10] Recently, many metal oxides have been widely investigated as anode materials for next-generation LIBs because of their natural abundance and high theoretical capacities.[5,11–15]

Tin oxide (SnO_2) stands out as one very attractive candidate considering its abundance, environmental benignity, and high theoretical capacity (780 $mAh\,g^{-1}$).[16,17] However, large volume variation (> 300 %) generally occurs in SnO_2-based materials during lithium insertion and extraction, which leads to pulverization and aggregation of electrochemically active particles, and formation of unstable solid–electrolyte interphase (SEI), thus resulting in rapid capacity fading.[18] To solve these problems, carbon-containing nanostructured materials including hollow and/or porous nanocomposites have been proposed to overcome the above challenges and received considerable attention.[19–21] The highly flexible carbon matrix could buffer the large mechanical strain during cycling, maintain the integrity of the whole electrode, and at the same time might increase the electrical conductivity. Moreover, hollow structures would better sustain the huge volume variation associated with lithium insertion/extraction, compared with solid counterparts. For example, various hollow structures, including nanotubes,[20,22–24] hollow nanospheres,[25–27] and nanocubes[11] have been prepared and demonstrated improved lithium storage performance especially with improved cycling stability.

A common drawback of these simple hollow structures is the low packing density of the materials compared to the solid counterparts, which originates from the large empty space within the particles. As a result, electrodes fabricated with these hollow spheres typically suffer from relatively low volumetric energy and power densities, which are undesirable for practical applications. To make better utilization of the inner hollow cavity, construction of complex hollow structures, such as yolk–shell or multi-shell hollow spheres could partly overcome the above-mentioned limitation of hollow particles.[28–30] Nevertheless, synthesis of complex hollow structures is generally challenging and complicated, and the shell structure should be carefully controlled to optimize the performance.[29]

Herein, we propose a novel yet simple strategy to increase the packing density of hollow particles by using bowl-like deflated hollow spheres. The as-prepared bowl-like SnO_2@carbon (SnO_2@C) particles with conformal carbon support inherit all advantages of hollow spheres, including the cavity to accommodate volume expansion upon lithium insertion and reduced distance for charge transport. More importantly, a bowl-like hollow structure excludes the unnecessary void space in conventional hollow particles, thus allowing the packing of more active materials per volume. As illustrated in Scheme 1, more bowl-like particles could be closely packed within a given amount of space compared to hollow spheres with the same diameter. Meanwhile, the void space in the bowl-like hollow structure would be still sufficient to accommodate the volume variation of the active material, which is similar to the spherical counterpart.

[*] J. Liang, H. Zhou, Prof. S. Ding
Department of Applied Chemistry, School of Science, MOE Key Laboratory for Nonequilibrium Synthesis and Modulation of Condensed Matter, State Key Laboratory for Mechanical Behavior of Materials, Xi'an Jiaotong University
Xi'an 710049 (China)
E-mail: dingsj@mail.xjtu.edu.cn
Dr. X.-Y. Yu, H. B. Wu, X. W. Lou
School of Chemical and Biomedical Engineering
Nanyang Technological University
62 Nanyang Drive, Singapore 637459 (Singapore)
E-mail: xwlou@ntu.edu.sg
Homepage: http://www.ntu.edu.sg/home/xwlou/

[**] This work was supported by the National Natural Science Foundation of China (No. 51273158, 21303131) and the Natural Science Basis Research Plan in Shaanxi Province of China (No. 2012JQ6003, 2013KJXX-49). X.W.L. acknowledges financial support from the Ministry of Education (Singapore) through the Academic Research Fund (AcRF) Tier-1 grant (RG12/13, M4011154). We thank Prof. Guang Yang and Dr. Chunhui Xiao for useful discussions.

Supporting information for this article is available on the WWW under http://dx.doi.org/10.1002/anie.201407917.

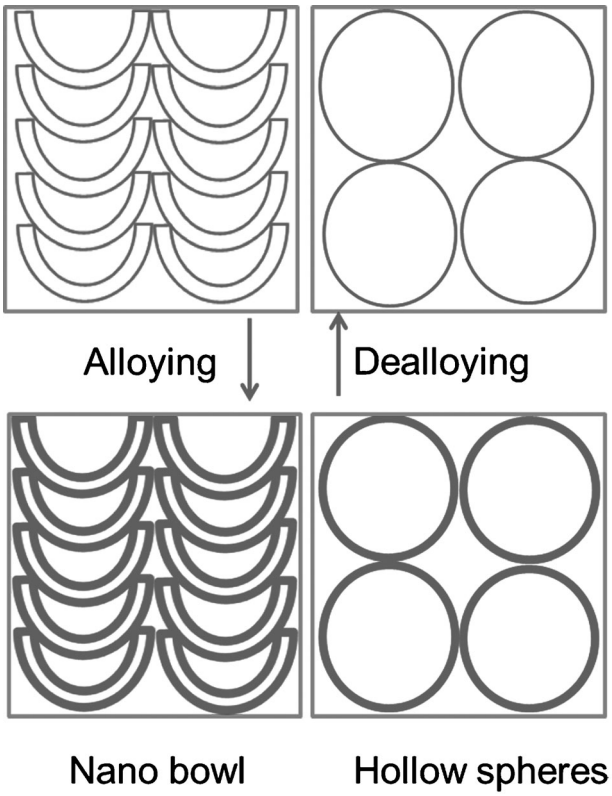

Scheme 1. Comparison of packing of bowl-like particles and spherical hollow particles and their participation in the charge–discharge process.

Subsequently, the volumetric capacity of as-fabricated electrodes would be substantially increased.

The formation procedure of the bowl-like SnO_2@C hybrid hollow nanostructure is shown in Scheme 2 (experimental details are given in the Supporting Information (SI)). First, an emulsion containing hollow polystyrene (PS) spheres[28,31] is dried in air to obtain deflated bowl-like structure due to the capillary force during the evaporation of solvent and the soft nature of PS thin shells. Second, the bowl-like PS particles serve as the template to support the deposition of a uniform SnO_2 layer via a simple precipitation reaction. Afterwards, the as-prepared bowl-like SnO_2@PS particles are treated in a nitrogen atmosphere at 550 °C for 4 h and converted into bowl-like SnO_2@C nanocomposite.

The morphology of the pristine hollow PS spheres is examined by field-emission scanning electron microscopy

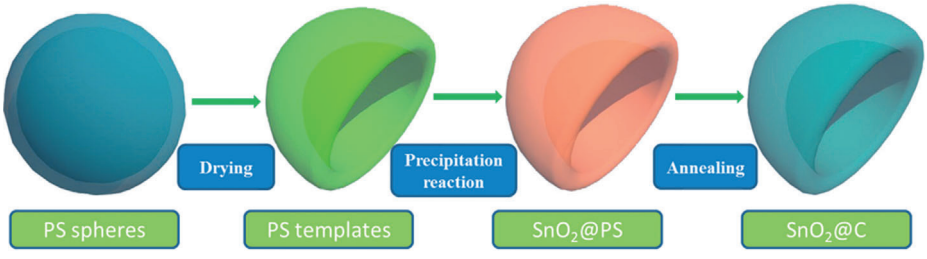

Scheme 2. Schematic illustration of the formation procedure of bowl-like SnO_2@C hollow particles.

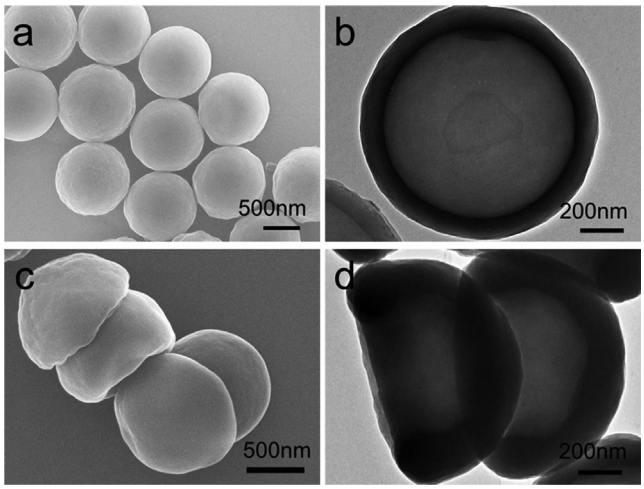

Figure 1. a, c) FESEM and b, d) TEM images of spherical PS hollow particles (a, b) and bowl-like PS particles (c, d).

(FESEM) and transmission electron microscopy (TEM) as shown in Figure 1 a,b. The pristine PS hollow spheres show high uniformity with diameter of about 1 μm and relatively smooth surface. After drying in air naturally, the pristine spherical particles are completely converted to deflated spheres with a bow-like morphology (Figure 1 c). Meanwhile the overall integrity of the particles is well preserved. TEM image (Figure 1 d) further reveals the well-defined cavity in the center of particles and complete merging of two layers of shell.

A SnO_2 layer is then uniformly coated on the surface of the PS templates via a facile solution-based method. The bowl-like structure is perfectly retained and the surface becomes slightly rougher (Figure 2 a and b). Moreover, the diameter of such SnO_2@PS particles increases to around 1.1 μm (Figure 2 c) owing to the deposition of SnO_2. After thermal treatment at 550 °C for 4 h in nitrogen, the bowl-like SnO_2@PS particles are converted into bowl-like SnO_2@C particles. The SnO_2@C particles well preserve the bowl-like shape (Figure 2 d), demonstrating the excellent structural stability. An enlarged view (Figure 2 e) reveals that the surface of SnO_2@C particles becomes quite rough and wrinkled compared to the pristine SnO_2@PS particles. This could be attributed to the carbonization of the PS templates and the generation of inner void space. TEM image (Figure 2 f) evidently suggests the unusual hollow structure. Because of the shrinkage of the shell during carbonization, the diameter of SnO_2@C particles reduces to about 900 nm. The selected area electron diffraction (SAED) pattern (Figure 2 g) indicates the polycrystalline nature of these bowl-like SnO_2@C particles and the diffraction rings can be readily assigned to the SnO_2 phase.[18] A representative high-resolution TEM (HRTEM) image is shown in Figure 2 h. The measured interplanar distance is

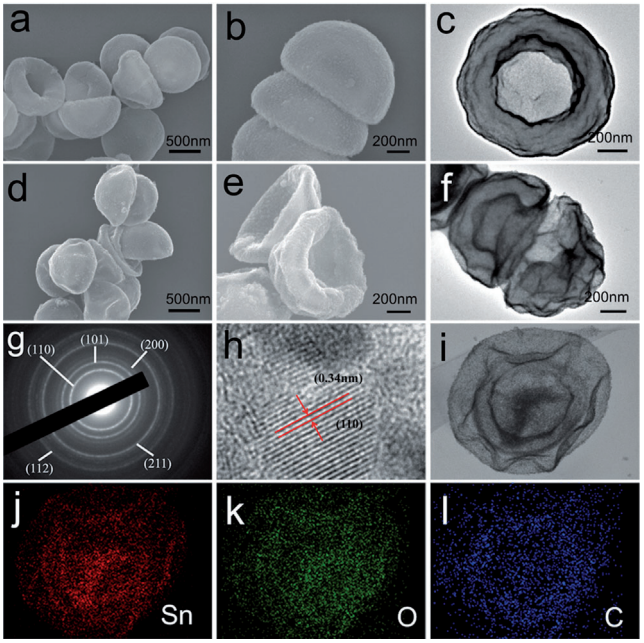

Figure 2. FESEM and TEM images of a–c) bowl-like SnO_2@PS particles and d–f) bowl-like SnO_2@C nanocomposite. g) SAED and h) HRTEM of bowl-like SnO_2@C nanocomposite. j–l) Elemental mapping images of an individual bowl-like SnO_2@C particle shown in (i).

0.34 nm, which matches well to the (110) plane of SnO_2.[32] To illustrate the spatial distribution of SnO_2 and carbon in the bowl-like SnO_2@C composite, energy-dispersive X-ray spectroscopy (EDX) elemental mapping is performed on a typical bowl-like SnO_2@C particle (Figure 2i). The result (Figure 2j–l) demonstrates the generally uniform distribution of Sn and C within the structure, which suggests the intimate contact between SnO_2 nanoparticles and the amorphous carbon matrix.

The weight fraction of SnO_2 in the nanocomposite is determined by themogravimetric analysis (TGA) as shown in Figure S1a (see SI). The TGA curve illustrates a significant weight loss at about 400 °C, which is attributed to combustion of the carbon component. After reaching 800 °C, the SnO_2@C sample shows a total weight loss of 23.7 %, corresponding to a SnO_2 content of 76.3 %. The crystallographic structure of the bowl-like SnO_2@C nanocomposite is characterized by powder X-ray diffraction (XRD), as shown in Figure S1b (see SI). The identified diffraction peaks can be perfectly assigned to rutile SnO_2, in good agreement with the JCPDS card No. 41-1445 ($P4_2/mnm$, $a_o = 4.738$ Å, $c_o = 3.187$ Å). No peaks of impurity such as Sn and SnO are found, which indicates the presence of only SnO_2 and amorphous carbon in the bowl-like SnO_2@C particles.[20] X-ray photoelectron spectroscopy (XPS) has been employed to analyze the bowl-like SnO_2@C nanocomposite (Figure S1c, see SI), further corroborating that Sn only exists in the form of SnO_2.[27] The porous characteristics of bowl-like SnO_2@C particles are further confirmed by nitrogen adsorption-desorption measurement. As shown in Figure S1d (see SI), the nitrogen adsorption–desorption isotherm of the product appears as a type IV with a relatively unusual type H4 hysteresis loop, suggesting a unique characteristic of large pores (the hollow interior) embedded in a matrix with pores of small sizes.[33] The pore size distribution (inset of Figure S1d) calculated by the Barrett–Joyner–Halenda (BJH) method corroborates the co-existence of nanopores of 2–3 nm in size and large pores over 50 nm. As expected, such a structure gives rise to a high Brunauer–Emmett–Teller (BET) specific surface area of about 103.8 $m^2 g^{-1}$.

Next, electrochemical measurements are carried out to evaluate the lithium storage properties of these bowl-like SnO_2@C particles. Figure 3a shows cyclic voltammograms (CV) curves of the first, second and fifth cycles of the electrode within the range of 0.005–3.0 V vs. Li/Li^+ at a scan rate of 0.5 $mV s^{-1}$. Two pronounced cathodic peaks at 0.6 and 0.07 V in the first cycle can be assigned to the initial reduction of SnO_2 to Sn [Eq. (1)] and formation of the SEI layer, and the alloying process to form Li_xSn [Eq. (2)], respectively.[34] During the first charging process, a strong peak at 0.7 and a broad peak at 1.24 V correspond to the de-alloying process from Li_xSn and partial reversible formation of SnO_2, respectively, which is in agreement with previous report.[35]

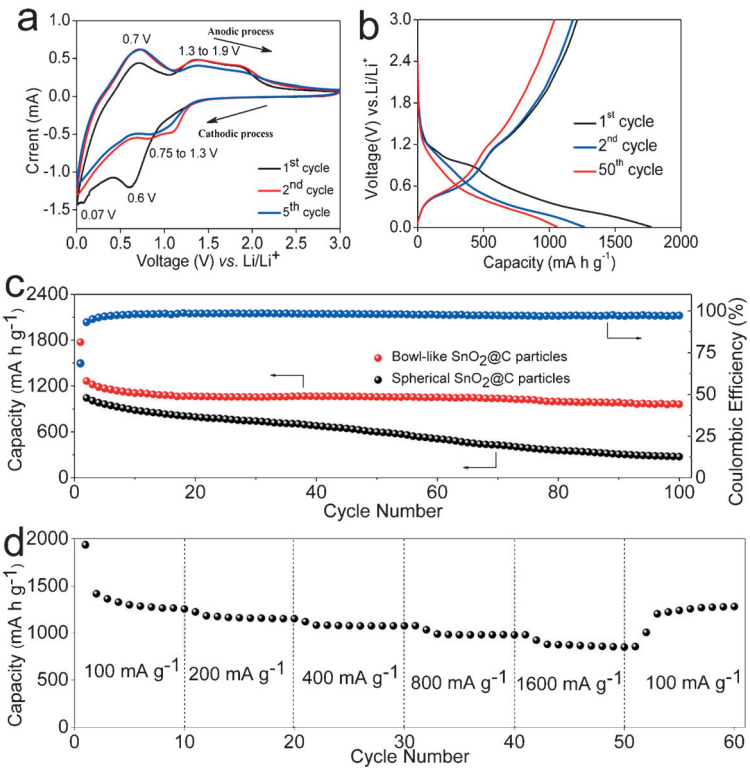

Figure 3. Electrochemical measurements of the bowl-like SnO_2@C nanocomposite: a) representative cyclic voltammograms (CVs) at a scan rate of 0.5 $mV s^{-1}$; b) charge–discharge voltage profiles for the 1st, 2nd, and 50th cycles at a current density of 400 $mA g^{-1}$; c) cycling performance at a current density of 400 $mA g^{-1}$ and the coulombic efficiency; d) rate performance.

$$SnO_2 + 4\,Li^+ + 4\,e^- \rightleftharpoons Sn + 2\,Li_2O \quad (1)$$

$$Sn + x\,Li^+ + x\,e^- \rightleftharpoons Li_xSn\ (0 \le x \le 4.4) \quad (2)$$

In the 2nd and 5th cycles, the peak at 0.62 V during cathodic scan shifts into a broad band from 0.75 to 1.30 V. Moreover, the CV curves of the 2nd and 5th cycles almost overlap, in support of the good reversibility of the electrochemical reactions in the electrode.

The electrochemical cycling stability of the bowl-like SnO_2@C particles is studied by galvanostatic charging/discharging in a voltage window of 0.05–3 V at a current density of 400 mA g^{-1}. As displayed in Figure 3b, poorly defined plateau regions can be observed in the charge–discharge profiles, consistent with the CV results. The initial discharge process leads to a very high initial capacity of 1772 mAh g^{-1}. The subsequent charge process delivers a capacity of 1212 mAh g^{-1}, leading to an initial loss of about 31.6% which is due to the formation of a SEI layer and the incomplete extraction of lithium from the active material. The discharge capacities of the 2nd and 50th cycles remain stable at 1263 and 1060 mAh g^{-1}, with the corresponding charge capacities of 1178 and 1040 mAh g^{-1}, respectively. Thus much higher Coulombic efficiency (CE) of 93.8% and 98.1% respectively can be obtained. Note that the specific capacity values are calculated based on the total mass of the bowl-like SnO_2@C nanocomposite, including the amorphous carbon support that typically shows negligible capacity. Figure 3c shows the cycling performance of the bowl-like SnO_2@C particles at a current density of 400 mA g^{-1} in a voltage window from 0.005 to 3 V vs. Li/Li$^+$. The discharge capacity slowly decreases to a value of about 963 mAh g^{-1} after 100 cycles, which is still significantly much higher than the theoretical capacity for graphite (372 mAh g^{-1}). It is worth mentioning that the capacity retention of the bowl-like SnO_2@C nanocomposite is significantly enhanced when compared with many other SnO_2 based nanostructures.[36–39] A post-mortem study shows that there is almost no change of the morphology after two charge–discharge cycles, and the bowl-like structure is somewhat retained after 100 cycles (Figure S2 and S3, see SI). Moreover, the bowl-like SnO_2@C nanocomposite can be cycled with high stability in a lower current density of 200 mA g^{-1} and a very high current density of 1600 mA g^{-1} (Figure S4, see SI). To make a further comparison, we have also investigated the electrochemical performance of spherical SnO_2@C hollow particles, which are prepared by the same procedure except for the pre-drying of hollow PS spheres (Figure S5, see SI). After 100 cycles at a current density of 400 mA g^{-1} between 0.005 and 3 V, the remaining capacity is only 97 mAh g^{-1} (Figure 3c), showing a fast capacity fading. The bowl-like SnO_2@C structure demonstrates satisfactory rate capability as well. As shown in Figure 3d, at increasing current densities of 100, 200, 400, 800 and 1600 mA g^{-1}, the bowl-like SnO_2@C nanocomposite shows high reversible specific capacities of about 1255, 1152, 1077, 981 and 850 mAh g^{-1}, respectively. It should be noted that, after the continuous cycling process with increasing current density, a specific capacity as high as 1282 mAh g^{-1} could be resumed at a current density of 100 mA g^{-1}, that is, about 90% retention of the reversible specific capacity in the second cycle. Such cycling performance and rate capability are remarkable compared with many literature reports of carbon-SnO_2 nanocomposites.

The attractive lithium storage properties of these bow-like SnO_2@C hybrid particles can be attributed to the following factors. First of all, the carbon-supported bow-like hollow structure completely inherits the advantages of conventional carbon-coated hollow structures, including the void space and conformal carbon layer to maintain the integrity of the electrode during charge–discharge cycling.[11,16] Secondly, the unique bow-like particles are expected to pack more densely as shown in Scheme 1 and Figure S6 (see SI). This unusual structural feature would make better utilization of the empty space of hollow particles, and thus improve the volumetric energy/power density of the electrode, which partly overcomes the low volumetric energy density drawback of conventional hollow particles. More importantly, such bow-like particles likely have more contact area with adjacent particles compared to spherical ones, leading to enhanced charge transport as well as better structural robustness of the electrode. In addition, it is interesting to note that the reversible capacity of SnO_2 in the bow-like SnO_2@C nanocomposite (e.g., ca. 1500 mAh g^{-1} at 400 mA g^{-1} based on the mass of SnO_2 assuming carbon is inactive) is close to the theoretical value of 1493 mAh g^{-1} assuming Equation (1) is completely reversible. Therefore, the high specific capacity of the bow-like SnO_2@C nanocomposite could be probably attributed to the improved reversibility of the reaction described by Equation (1). Moreover, the reversible formation of gel-like film[10,19,38,40–45] and the interfacial storage of additional charge between the primary nanoparticles[46,47] might also contribute to the high specific capacity, which have been observed in many metal oxide electrode materials.

In summary, we have developed a facile and efficient method to synthesize bowl-like SnO_2@C hollow particles as a high-performance anode material for lithim-ion batteries. The unique architecture, which not only retains the advantages of conventional hollow structures but also brings additional benefits such as the increased packing density and improved interconnection of the particles, is the key factor to remarkably improve the electrochemical performance. Impressively, the resultant bowl-like SnO_2@C hollow nanocomposite manifests a high specific capacity with enhanced cycling stability. The concept demonstrated here may help pave the way for practical use of hollow particles in next-generation lithium-ion batteries.

Received: August 3, 2014
Published online: September 22, 2014

Keywords: anode materials · hollow nanostructures · lithium-ion batteries · nanobowls · SnO_2

[1] P. G. Bruce, B. Scrosati, J. M. Tarascon, *Angew. Chem. Int. Ed.* **2008**, *47*, 2930–2946; *Angew. Chem.* **2008**, *120*, 2972–2989.
[2] Y. Idota, T. Kubota, A. Matsufuji, Y. Maekawa, T. Miyasaka, *Science* **1997**, *276*, 1395–1397.
[3] J.-M. Tarascon, M. Armand, *Nature* **2001**, *414*, 359–367.

[4] J. S. Chen, X. W. Lou, *Small* **2013**, *9*, 1877 – 1893.
[5] W. Zhou, C. Cheng, J. Liu, Y. Y. Tay, J. Jiang, X. Jia, J. Zhang, H. Gong, H. H. Hng, T. Yu, *Adv. Funct. Mater.* **2011**, *21*, 2439 – 2445.
[6] Y. Wang, Y. Wang, E. Hosono, K. Wang, H. Zhou, *Angew. Chem. Int. Ed.* **2008**, *47*, 7461 – 7465; *Angew. Chem.* **2008**, *120*, 7571 – 7575.
[7] Y. G. Guo, Y. S. Hu, W. Sigle, J. Maier, *Adv. Mater.* **2007**, *19*, 2087 – 2091.
[8] G. Derrien, J. Hassoun, S. Panero, B. Scrosati, *Adv. Mater.* **2007**, *19*, 2336 – 2340.
[9] X. W. Lou, J. S. Chen, P. Chen, L. A. Archer, *Chem. Mater.* **2009**, *21*, 2868 – 2874.
[10] W. M. Zhang, X. L. Wu, J. S. Hu, Y. G. Guo, L. J. Wan, *Adv. Funct. Mater.* **2008**, *18*, 3941 – 3946.
[11] L. Zhang, H. B. Wu, B. Liu, X. W. Lou, *Energy Environ. Sci.* **2014**, *7*, 1013 – 1017.
[12] L. Liu, Y. Guo, Y. Wang, X. Yang, S. Wang, H. Guo, *Electrochim. Acta* **2013**, *114*, 42 – 47.
[13] Z. Wang, L. Zhou, X. W. Lou, *Adv. Mater.* **2012**, *24*, 1903 – 1911.
[14] C. W. Lee, S.-D. Seo, D. W. Kim, S. Park, K. Jin, D.-W. Kim, K. S. Hong, *Nano Res.* **2013**, *6*, 348 – 355.
[15] L. Zhou, H. B. Wu, Z. Wang, X. W. Lou, *ACS Appl. Mater. Interfaces* **2011**, *3*, 4853 – 4857.
[16] X. W. Lou, C. M. Li, L. A. Archer, *Adv. Mater.* **2009**, *21*, 2536 – 2539.
[17] C. Wang, Y. Zhou, M. Ge, X. Xu, Z. Zhang, J. Jiang, *J. Am. Chem. Soc.* **2010**, *132*, 46 – 47.
[18] D. Wang, J. Yang, X. Li, D. Geng, R. Li, M. Cai, T.-K. Sham, X. Sun, *Energy Environ. Sci.* **2013**, *6*, 2900 – 2906.
[19] X. Li, X. Meng, J. Liu, D. Geng, Y. Zhang, M. N. Banis, Y. Li, J. Yang, R. Li, X. Sun, *Adv. Funct. Mater.* **2012**, *22*, 1647 – 1654.
[20] Y. Wang, H. C. Zeng, J. Y. Lee, *Adv. Mater.* **2006**, *18*, 645 – 649.
[21] X. Huang, X. Zhou, L. Zhou, K. Qian, Y. Wang, Z. Liu, C. Yu, *ChemPhysChem* **2011**, *12*, 278 – 281.
[22] X. Xu, J. Liang, H. Zhou, D. Lv, F. Liang, Z. Yang, S. Ding, D. Yu, *J. Mater. Chem. A* **2013**, *1*, 2995 – 2998.
[23] Z. Wen, Q. Wang, Q. Zhang, J. Li, *Adv. Funct. Mater.* **2007**, *17*, 2772 – 2778.
[24] J. Ye, H. Zhang, R. Yang, X. Li, L. Qi, *Small* **2010**, *6*, 296 – 306.
[25] S. Ding, J. S. Chen, G. Qi, X. Duan, Z. Wang, E. P. Giannelis, L. A. Archer, X. W. Lou, *J. Am. Chem. Soc.* **2011**, *133*, 21 – 23.
[26] X. W. Lou, Y. Wang, C. Yuan, J. Y. Lee, L. A. Archer, *Adv. Mater.* **2006**, *18*, 2325 – 2329.
[27] Y.-S. Lin, J.-G. Duh, M.-H. Hung, *J. Phys. Chem. C* **2010**, *114*, 13136 – 13141.
[28] M. Yang, J. Ma, C. Zhang, Z. Yang, Y. Lu, *Angew. Chem. Int. Ed.* **2005**, *44*, 6727 – 6730; *Angew. Chem.* **2005**, *117*, 6885 – 6888.
[29] J. Wang, N. Yang, H. Tang, Z. Dong, Q. Jin, M. Yang, D. Kisailus, H. Zhao, Z. Tang, D. Wang, *Angew. Chem. Int. Ed.* **2013**, *52*, 6417 – 6420; *Angew. Chem.* **2013**, *125*, 6545 – 6548.
[30] G. Zhang, X. W. Lou, *Angew. Chem. Int. Ed.* **2014**, *53*, 1516 – 1520; *Angew. Chem.* **2014**, *126*, 1542 – 1546.
[31] M. Yang, J. Ma, Z.-w. Niu, X. Dong, H. Xu, Z. Meng, Z. Jin, Y. Lu, Z. Hu, Z. Yang, *Adv. Funct. Mater.* **2005**, *15*, 1523 – 1528.
[32] H. Wang, A. L. Rogach, *Chem. Mater.* **2014**, *26*, 123 – 133.
[33] M. Kruk, M. Jaroniec, *Chem. Mater.* **2001**, *13*, 3169 – 3183.
[34] J. C. Lytle, H. Yan, N. S. Ergang, W. H. Smyrl, A. Stein, *J. Mater. Chem.* **2004**, *14*, 1616 – 1622.
[35] X. Zhang, J. Liang, G. Gao, S. Ding, Z. Yang, W. Yu, B. Q. Li, *Electrochim. Acta* **2013**, *98*, 263 – 267.
[36] Q. Tian, Z. Zhang, J. Chen, L. Yang, S.-i. Hirano, *J. Power Sources* **2014**, *246*, 587 – 595.
[37] P. Lian, J. Wang, D. Cai, L. Ding, Q. Jia, H. Wang, *Electrochim. Acta* **2014**, *116*, 103 – 110.
[38] X. Zhou, L. J. Wan, Y. G. Guo, *Adv. Mater.* **2013**, *25*, 2152 – 2157.
[39] H. B. Wu, J. S. Chen, X. W. Lou, H. H. Hng, *J. Phys. Chem. C* **2011**, *115*, 24605 – 24610.
[40] A. L. M. Reddy, M. M. Shaijumon, S. R. Gowda, P. M. Ajayan, *Nano Lett.* **2009**, *9*, 1002 – 1006.
[41] L.-F. Cui, Y. Yang, C.-M. Hsu, Y. Cui, *Nano Lett.* **2009**, *9*, 3370 – 3374.
[42] A. Magasinski, P. Dixon, B. Hertzberg, A. Kvit, J. Ayala, G. Yushin, *Nat. Mater.* **2010**, *9*, 353 – 358.
[43] Y. Sun, X. Hu, W. Luo, F. Xia, Y. Huang, *Adv. Funct. Mater.* **2013**, *23*, 2436 – 2444.
[44] X. Liu, S. W. Or, C. Jin, Y. Lv, C. Feng, Y. Sun, *Carbon* **2013**, *60*, 215 – 220.
[45] D. Xie, Q. Su, Z. Dong, J. Zhang, G. Du, *CrystEngComm* **2013**, *15*, 8314 – 8319.
[46] K. Zhong, B. Zhang, S. Luo, W. Wen, H. Li, X. Huang, L. Chen, *J. Power Sources* **2011**, *196*, 6802 – 6808.
[47] X. Yu, Y. He, J. Sun, K. Tang, H. Li, L. Chen, X. Huang, *Electrochem. Commun.* **2009**, *11*, 791 – 794.

